Applied Catalysis B: Environmental 226 (2018) 523–533

Contents lists available at ScienceDirect

Applied Catalysis B: Environmental

journal homepage: www.elsevier.com/locate/apcatb

Nitrogen-doped carbon-decorated copper catalyst for highly efficient transfer hydrogenolysis of 5-hydroxymethylfurfural to convertibly produce 2,5-dimethylfuran or 2,5-dimethyltetrahydrofuran

Zhi Gao, Chenyue Li, Guoli Fan, Lan Yang, Feng Li*

State Key Laboratory of Chemical Resource Engineering, Beijing Advanced Innovation Center for Soft Matter Science and Engineering, Beijing University of Chemical Technology, Beijing, 100029, PR China

ARTICLE INFO

Keywords:
Nitrogen-doped carbon
Copper-based nanocatalyst
Catalytic transfer hydrogenolysis
5-hydroxymethylfurfural
Biomass transformation

ABSTRACT

Currently, highly efficient transformation of abundant and low-cost renewable raw biomass into high-quality biofuels and important chemicals is one of the most promising solutions to the current energy crisis, rapid consumption of fossil resources, increasing emission of greenhouse gases and serious environmental pollution. Here, convertible production of promising 2,5-dimethylfuran (DMF) and 2,5-dimethyltetrahydrofuran (DMTHF) biofuels was achieved successfully via green catalytic transfer hydrogenolysis of biomass-derived 5-hydroxymethylfurfural (HMF) using a nitrogen-doped carbon (NC)-decorated copper-based catalyst with cyclohexanol as hydrogen source. DMF or DMTHF with high yield of 96.1% or 94.6% was produced convertibly through simply modulating reaction time. Extensive characterizations revealed that appropriate surface base sites on the catalyst could efficiently promote the activation of alcohol hydroxyl in cyclohexanol and the subsequent release of active hydrogen species, while highly dispersed surface Cu^0 nanoparticles and electrophilic Cu^+ species were beneficial to the hydrogen transfer and the activation of both the carbonyl group and the hydroxyl group in HMF, respectively. Moreover, as-fabricated NC-decorated Cu-based catalyst presented high stability without obvious loss of catalytic performance after five consecutive cycles, due to the strong interaction between the support and active metal species. Such non-noble metal catalyst has a promising industrial application in the production of valuable biomass fuels.

1. Introduction

With the rapid depletion of non-renewable petroleum-based reserves and the resulting problems arising from increasing emission of greenhouse gases and environmental pollution, abundant and low-cost renewable raw biomass, as a promising alternative to fossil resources for the sustainable production of important chemicals and fuels, is attracting more and more attention in both industry and academia communities [1,2]. For instance, 5-hydroxymethylfurfural (HMF) derived from inedible lignocellulose is perceived as one of the most important key platform molecules in the manufacturing of high value-added chemicals and biofuels [3–6]. Especially, HMF hydrogenolysis can further produce 2,5-dimethylfuran (DMF) and 2,5-dimethyltetradyrofuran (DMTHF) [7]. Due to their fabulous properties (*e.g.* high energy densities, good combustibility and low volatility), DMF and DMTHF are utilized widely as suitable biomass-derived liquid fuels or additives [8]. Additionally, DMTHF also can serve as a potential alternative to traditional tetrahydrofuran solvent [9]. Besides DMF and DMTHF, other various compounds, such as 5-methylfurfural (5-MF), 5-methylfurfuryl alcohol (5-MFA), 2,5-bis(hydroxymethyl) furan (BHMF) and 2,5-bis(hydroxymethyl)tetrahydrofuran (DHTHF) can be generated by hydrogenating HMF with several functional groups (i.e. C═O, C═C, C—O and furan ring). Thus, highly efficient conversion of HMF to DMF and DMTHF, i.e. selective C-O bond cleavage, remains a huge challenge.

To date, various heterogeneous noble metal (*e.g.* Pt [10,11], Ru [12–14] and Pd [15–17]) catalysts have been applied for the HMF hydrogenolysis. However, some drawbacks of high cost, easy deactivation and difficulty in the regeneration limit their scale-up applications. Therefore, low-cost non-noble metal catalysts is attracting great interest in the above reaction process. Recently, many efforts have been drawn towards nickel- and copper-based catalysts [18–24], such as Ni-Al_2O_3 [18], Ni-nickel phyllosilicate [19], Ni-W_2C/AC [20], Cu-Zn alloy [22], and bimetallic Cu-Co [23,24]. In most cases, they show relatively high conversions and selectivities to DMF or DMTHF in the presence of molecular hydrogen under harsh reactions conditions (e.g. high

* Corresponding author.
E-mail address: lifeng@mail.buct.edu.cn (F. Li).

https://doi.org/10.1016/j.apcatb.2018.01.006
Received 16 October 2017; Received in revised form 11 December 2017; Accepted 3 January 2018
Available online 04 January 2018
0926-3373/

hydrogen pressure and long reaction time). Even so, high cost of hydrogen transportation and storage and flammability of hydrogen are unfavorable factors in practical applications [25]. Currently, noble metal-catalyzed transfer hydrogenation/hydrogenolysis of HMF using non-corrosive alcohols as hydrogen donors has emerged as an alternative to conventional hydrogenation using molecular hydrogen [26–29]. In this regard, developing cost-effective and high-performance non-noble metal catalysts is a highly meaning work.

As a family of important two-dimensional layered clay materials, layered double hydroxides (LDHs) with different metal M^{2+} and M^{3+} cations uniformly distributed and orderly prearranged in the brucite-like layers can be transformed into highly dispersed metal nanoparticles (NPs) over mixed metal oxides (MMOs) [30–33]. In particular, MMOs as wonderful supports can provide abundant surface Lewis basic sites, which are beneficial to a wide variety of base-catalyzed reactions [34–37]. Recently, our group has reported that copper NPs supported over LDH-derived CaAl-MMO with strong basicity exhibited excellent catalytic dehydrogenation property [38]. On the other side, nitrogen-doped carbon (NC) materials have received considerable attention in recent years [39–42]. Especially, doping electron-rich nitrogen into the carbon architecture can significantly change the physical and chemical properties of carbon materials [43–46], which makes NC an ideal support material in nanocatalysis [47,48]. What's more, strong electronic interactions between the NC and active species can greatly improve the stability of resulting catalysts.

In this present work, the combination of LDH and melamine was performed and correspondingly, a robust, low-cost and sustainable NC-decorated copper-based catalyst (NC-Cu/MgAlO) was rationally fabricated by a simple thermal decomposition of hybrid CuMgAl-LDH/melamine precursor (Scheme 1) and applied for the catalytic transfer hydrogenolysis of HMF to produce DMF or DMTHF using cyclohexanol as both the hydrogen honor and the solvent. It was found that surface NC decoration led to the increase in the amount of accessible base sites on the catalyst surface, and extremely high yields of DMF (96.1%) and DMTHF (94.6%) were diversely achieved only by simply modulating reaction time. As far as my knowledge, this is the first report about such highly efficient non-noble copper-catalyzed transfer hydrogenolysis of HMF to convertibly produce DMF or DMTHF.

2. Experimental

2.1. Catalyst preparation

CuMgAl-LDH/melamine composite precursor was prepared by a coprecipitation method. A salt solution containing $Cu(NO_3)_2{\cdot}3H_2O$ (0.1 M), $Mg(NO_3)_2{\cdot}6H_2O$ (0.1 M), $Al(NO_3)_3{\cdot}9H_2O$ (0.1 M) and melamine (0.3 M) dissolved in 100 mL deionized water was titrated by a mixed base solution of NaOH (0.48 M) and Na_2CO_3 (0.2 M) under vigorous agitation at room temperature until the pH value of solution reached 10.0. Then the suspension was aged at 70 °C for 10 h, and centrifuged. The obtained precipitate was washed with deionized water for several times. Subsequently, the obtained CuMgAl-LDH/melamine precursor was dried at 70 °C overnight and then calcined in static air at 600 °C for 6 h to obtain NC-CuMgAlO. At last, NC-CuMgAlO was reduced at 350 °C in 10% H_2/Ar atmosphere for 2 h with a ramping rate of 2 °C/min to obtain reduced NC-Cu/MgAlO sample. In addition, NC-MgAlO support was also prepared using the above same procedure without the addition of $Cu(NO_3)_2{\cdot}3H_2O$.

For comparison, CuMgAl-LDH, CuAl-LDH/melamine and CuMg/melamine were synthesized using the above identical procedure without the addition of melamine, $Mg(NO_3)_2{\cdot}6H_2O$ and $Al(NO_3)_3{\cdot}9H_2O$, respectively, and the resulting calcined or reduced samples were denoted as CuMgAlO or Cu/MgAlO, NC-CuAlO or NC-Cu/Al_2O_3, and NC-CuMgO or NC-Cu/MgO, respectively.

2.2. Characterization

X-ray diffraction (XRD) patterns were recorded using a Shimadzu XRD-6000 diffractometer. Cu Kα radiation (λ = 0.15418 nm, 40 kV, 30 Ma) was used as an X-ray source. The crystal size was calculated using the scherrer equation through the Cu (111) diffraction peak.

Elemental analysis was conducted on a Shimadzu ICPS-7500 inductively coupled plasma atomic emission spectroscopy (ICP-AES) after the samples were dissolved in nitrohydrochloric acid. The contents of carbon and nitrogen were determined by elemental microanalysis (Elementar Vario analyzer).

Low temperature N_2 adsorption–desorption isotherms were recorded using a Micromeritics ASAP 2020 sorptometer apparatus. Before measurements, the samples were outgassed at 100 °C for 4 h. The specific surface areas were obtained using the Brunauer – Emmett – Teller (BET) method. The average pore volume and pore size were determined by Barrett – Joyner – Halenda (BJH) method.

Transmission electron microscopy (TEM) and high-resolution TEM (HRTEM) images were taken using a JEOL 2100 microscope operated at an accelerating voltage of 200 kV. The samples were dispersed in ethanol under supersonic waves and then placed on carbon film before measurements.

High-angle annular dark-field scanning TEM-energy-dispersive X-ray spectroscopy (HAADF-STEM-EDX) images were recorded on a JEOL2010F instrument.

Hydrogen temperature-programmed reduction (H_2-TPR) was carried out using a Micromeritics ChemiSorb 2920 instrument. In a typical experiment, the samples placed in a quartz U-tube reactor were pretreated in an argon flow (40 ml/min) at 200 °C for 1 h. Then, the TPR analysis was carried out in in a stream of 10% v/v H_2/Ar (40 mL/min) with a heating rate of 5 °C min^{-1} up to 800 °C. The effluent gas was analyzed by a thermal conductivity detector (TCD).

Temperature-programmed desorption of CO_2 (CO_2-TPD) was used to explore the basic properties of samples. The experiments were conducted in Micromeritics ChemiSorb 2920 instrument. Firstly, the samples were placed in a quartz U-tube reactor and pretreated in an argon flow (40 ml/min) at 200 °C for 1 h. Then, the CO_2 gas flow (40 ml/min) was introduced into the samples at 50 °C for 1 h. Subsequently, the physisorbed CO_2 was flushed off under argon flow (40 ml/min) at 50 °C for 1 h. Finally, the chemisorbed CO_2 was desorbed by raising the temperature from 50 °C to 900 °C and detected using a thermal conductivity detector (TCD).

Temperature programmed desorption of NH_3 (NH_3–TPD) experiments were performed on the AutoChem II. 2920 instrument (Micromeritics, USA). Prior to the tests, the sample (0.1 g) was pretreated in a He flow (40 ml/min) at 400 °C for 1 h. After cooling to about 50 °C, the sample was saturated under a NH_3 flow for 1 h and

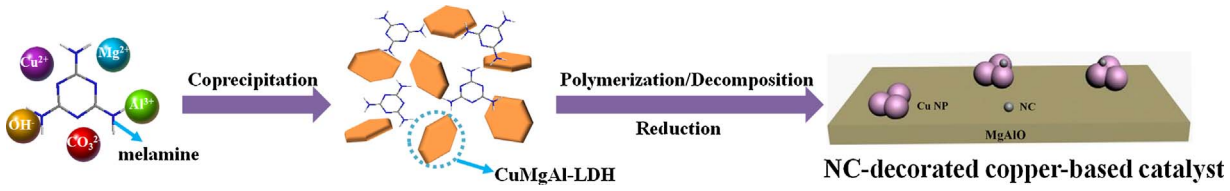

Scheme 1. The synthetic procedure for NC-Cu/MgAlO through thermal decomposition of hybrid CuMgAl-LDH/melamine precursor.

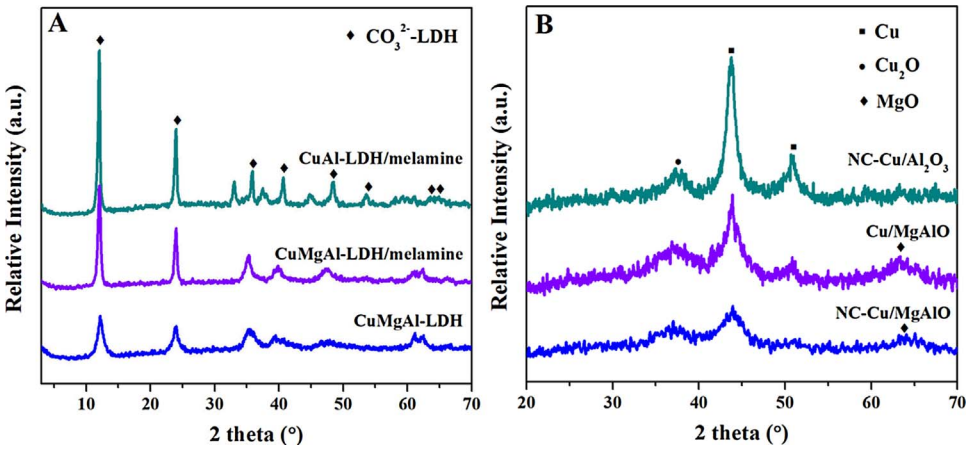

Fig. 1. XRD patterns of different precursors (A) and reduced samples (B).

Table 1
Structural and textural data for different catalysts.

Catalyst	Content (wt.%)			S_{BET}[c] (m^2/g)	V_{pore}[d] (cm^3/g)	D_p[e] (nm)	D_{111}[f] (nm)	S_{Cu}[g] (m^2/g)	$Cu^+/(Cu^0 + Cu^+)$ ratio[h]
	Cu[a]	C[b]	N[b]						
NC-MgAlO	0	8.0	0.45	116	0.8	19.2	–	–	–
NC-Cu/MgAlO	31.6	7.2	0.42	136	0.28	6.1	5.8	29.7	0.54
Cu/MgAlO	32.5	0	0	92	0.20	7.4	7.6	26.5	0.41
NC-Cu/Al_2O_3	42.7	4.6	0.5	77	0.15	7.1	11.7	18.2	0.46

[a] Determined by ICP-AES.
[b] Determined by elemental microanalysis.
[c] Specific surface area calculated by the BET method.
[d] Total pore volume.
[e] Mean pore diameter.
[f] Average crystallite size of metallic Cu particles based on XRD patterns.
[g] Metallic Cu surface area determined by N_2O titration.
[h] Determined by XAES analysis.

then purged with a He flow (40 ml/min) for 1 h. At last, the sample was heated to 500 °C at a rate of 10 °C/min.

In situ infrared (IR) spectra of pyridine adsorbed on samples were obtained using Thermo Nicolet 380 spectrometer. Firstly, the sample (50 mg) was pressed into a very thin self-supporting wafer. The disc was mounted in an evacuable quartz IR cell with a CaF_2 window. Then, the sample was pretreated at 200 °C under Ar flow for 1 h and cooled down to room temperature. Afterwards, pyridine was introduced and held for 1 h. Finally, IR spectra of pyridine adsorption were collected under vacuum at 20 °C.

The copper surface areas of samples were obtained through H_2-N_2O titration using a Micromeritics ChemiSorb 2920 instrument. Firstly, the calcined samples underwent H_2-TPR in 10% v/v H_2/Ar (40 mL/min) from 50 °C to 300 °C and then kept at 300 °C until no more H_2 was consumed. After cooling down the temperature to 60 °C, the gas was switched to 10% N_2O/N_2 to oxide the surface Cu atoms, followed by Ar purging and cooling the sample to room temperature. Finally, H_2-TPR was performed again under 10% v/v H_2/Ar (40 mL/min) to 300 °C. Cu surface area was calculated by assuming a spherical shape of the Cu metal particles and a surface concentration of 1.47×1019 Cu atoms m^{-2}.

X-ray photoelectron spectroscopy (XPS) and X-ray-induced Auger electron spectroscopy (XAES) spectra were obtained using a Thermo VG ESCALAB250 X-ray photoelectron spectrometer. Al Kα radiation (1486.6 eV photons) was used as an X-ray source. In order to minimize the influence of radiation used on the chemical states of copper species, probably resulting in the photoreduction of copper oxide species in the spectrometer, the sample was initiated by a single-scan analysis of the Cu 2p region (no more than 20 second) or Cu LMM (no more than 1 min) in the course of XPS and XAES experiments. All of the binding energies were corrected by C 1 s and the binding energy of C-C is 284.6 eV.

2.3. Catalyst test

Typical procedure for the liquid phase transfer HMF hydrogenolysis: HMF (0.5 g), the catalyst (0.1 g) and cyclohexanol (10 mL) were mixed in a stainless-steel autoclave (100 mL) equipped with a magnetic stirrer. After purging with 2 MPa N_2 for 10 times, the reactor was conducted under N_2 at atmospheric pressure at the required temperature for a desired time with magnetic stirring. After the reaction, the autoclave was cooled with an ice-water bath and depressurized carefully. Finally, the liquid products were analyzed by an Agilent GC7890 B gas chromatograph equipped with flame ionization detector and DB-wax capillary column (30.0 m × 250 μm × 0.25 μm) and identified as compared with known standards using tridecane as an internal standard. In all cases, the carbon balances were above 96%. The injector temperature was set at 250 °C, and the detector column temperature was increased from 100 to 150 °C with a ramp rate of 5 °C min^{-1}. The experimental errors for the conversions and selectivities were less than 3% obtained according to at least 3 parallel experiments.

3. Results and discussion

3.1. Structural analysis of samples

As shown in Fig. 1A, XRD patterns of three CuAl-LDH/melamine, CuMgAl-LDH/melamine and CuMgAl-LDH precursor samples all exhibit characteristic diffractions indexed to (003), (006), (012), (015), (018), (110) and (113) crystalline planes of hydrotalcite-like materials. No

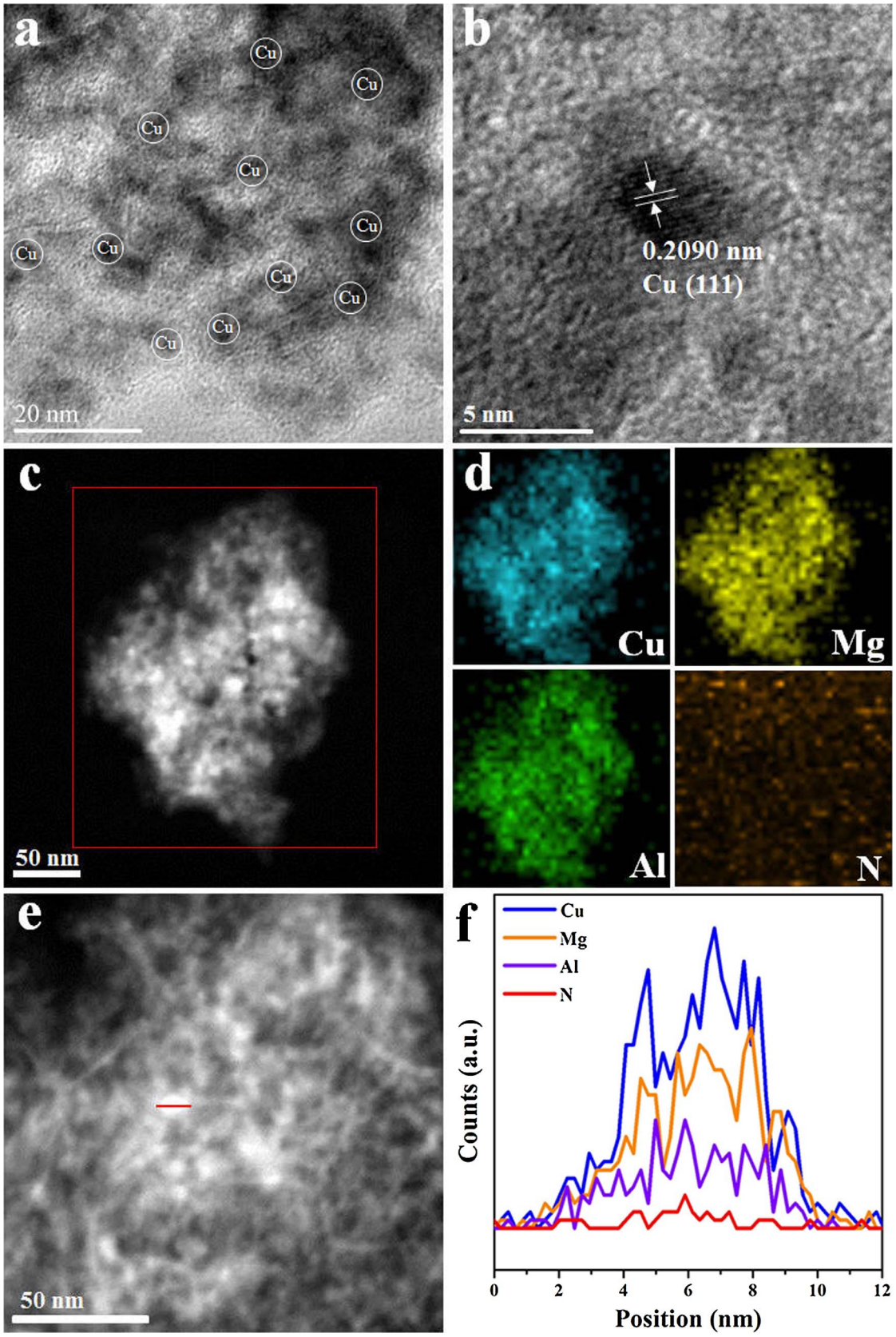

Fig. 2. HRTEM images (a and b) of NC-Cu/MgAlO sample. HAADF–STEM image (c) of NC-Cu/MgAlO with the EDX mapping (d); high-magnification STEM image (e); EDX line spectra of Cu-*K*, Mg-*L*, Al-*K* and N-*K* along the red line in e (f). (For interpretation of the references to colour in this figure legend, the reader is referred to the web version of this article.)

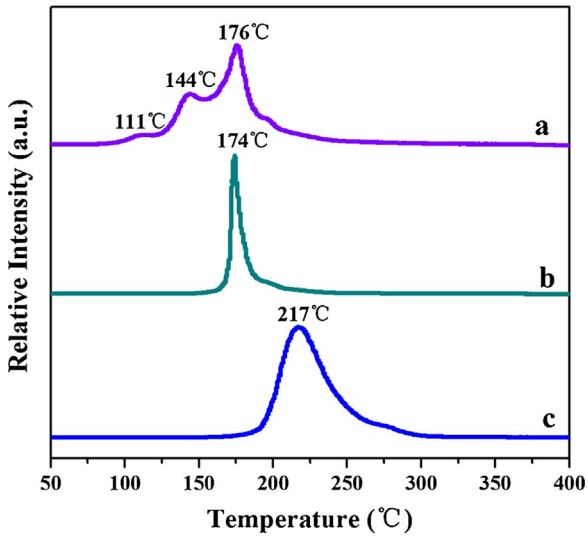

Fig. 3. H_2-TPR profiles of calcined CuMgAlO (a), NC-CuMgAlO (b) and NC-CuAlO (c) samples.

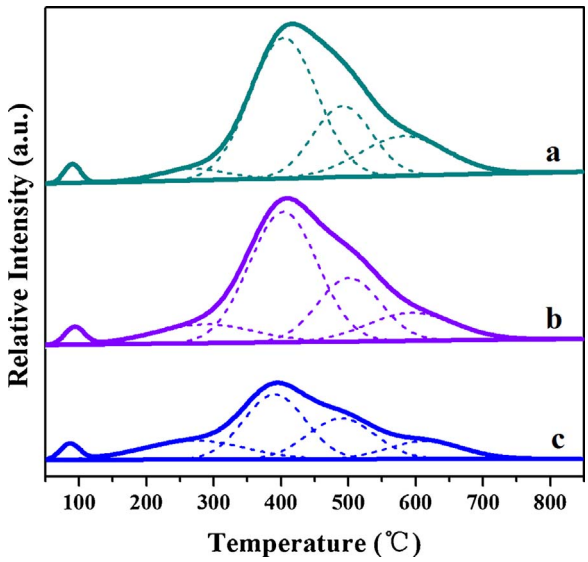

Fig. 4. CO_2-TPD profiles of NC-Cu/MgAlO (a), Cu/MgAlO (b) and NC-Cu/Al_2O_3 (c) samples.

Table 2
Quantitative analysis of surface basic sites over different Cu-based samples.

Catalyst	Specific basicity (CO_2 μmol g^{-1})[a]				
	Total	W.	M.	S.	SS.
NC-Cu/MgAlO	384.0	6.9 (1.8)[b]	16.5 (4.3)	287.6 (74.9)	73.0 (19.0)
Cu/MgAlO	355.6	6.8 (1.9)	38.0 (10.7)	261.0 (73.4)	49.8 (14)
NC-Cu/Al_2O_3	239.2	6.9 (2.9)	44.7 (18.7)	156.2 (65.3)	31.4 (13.1)

[a] W.: weak basic sites; M.: medium-strength basic sites; S.: strong basic sites; SS.: super strong basic sites.

[b] Relative amounts of the basic sites (%).

diffractions related to melamine can be observed, mainly owing to the small content of high dispersive melamine in samples. All reduced Cu-based samples present characteristic diffractions of metallic Cu and Cu_2O phases, besides MgO phase detected in Mg-containing Cu/MgAlO and NC-Cu/MgAlO samples (Fig. 1B). Meanwhile, no crystalline Al_2O_3 can be observed in each case, suggesting that aluminum in reduced Cu-based samples may exist either in the form of amorphous alumina or in the form of mixed metal MgAlO oxides (e.g. MgO-like phase). Therefore, such Al-containing components can act as both the support and the physical spacer to enhance metal–support interactions, inhibit the aggregation of Cu NPs and improve the dispersion of Cu NPs. As listed in Table 1, the average particle size of Cu NPs in the NC-Cu/MgAlO estimated according to Scherrer equation is smaller than those in NC-Cu/Al_2O_3 and Cu/MgAlO samples, while the Cu surface area measured by H_2-N_2O titration in the NC-Cu/MgAlO is higher than those in NC-Cu/Al_2O_3 and Cu/MgAlO samples. This result demonstrates that the introduction of Mg and melamine into the catalyst precursor is helpful to retarding the growth of metallic Cu crystallites. In addition, it is noted from Table 1 that the specific surface area of NC-Cu/MgAlO sample can reach 136 $m^2 g^{-1}$, which is the highest among them.

The morphology and microstructure of NC-Cu/MgAlO were elucidated by SEM and TEM characterizations. The representative SEM image (Fig. S1) demonstrates the blocky morphology of the sample, and typical TEM micrographs of samples (Fig.S2) depict highly dispersed black Cu NPs on the surface of NC-Cu/MgAlO and Cu/MgAlO. However, serious agglomeration of Cu NPs is especially observed in the NC-Cu/MgO. The average size of Cu NPs over the NC-Cu/MgAlO (4.59 nm) is smaller than those over Cu/MgAlO (6.34 nm), NC-Cu/Al_2O_3 (10.56 nm) and NC-Cu/MgO (12.45 nm), respectively.

Further, HRTEM images of NC-Cu/MgAlO also depict that Cu NPs are well dispersed on the support (Fig. 2a). Moreover, a typical HRTEM image (Fig. 2b) reveals that one single particle possesses clear lattice fringes with the interplanar spacings of about 2.09 Å, which is indexed to the (111) plane of metallic copper phase. And, uniform special distributions of Cu, Mg, Al and N elements can be observed from the EDS mapping of HAADF-STEM image (Fig. 2c and d), while the STEM-EDX line scan spectra clearly illustrate similar distributions of Cu, Mg, Al and N elements along one particle (Fig. 2e and f), reflecting the character of their close contact.

3.2. Redox behaviors and surface properties of samples

To investigate the nature of metal-support interaction and the formation of active metal sites in calcined samples, H_2-TPR experiments were performed. As for NC-free CuMgAlO (Fig. 3a), a broad peak centered at about 176 °C, along with two small shoulders at 111 °C and 144 °C, is associated with the reduction of surface isolated highly dispersed Cu^{2+} species. With the introduction of melamine, NC-CuMgAlO only presents a sharp peak at about 174 °C (Fig. 3b), indicative of the existence of stronger interaction between Cu species and the support. Such interaction can lead to the relatively poorer reducibility of Cu^{2+} species. In contrast to NC-CuMgAlO, Mg-free NC-CuAlO sample presents a peak at the higher temperature of 217 °C (Fig. 3c), demonstrating that the introduction of Mg is good for the improvement in the dispersion of Cu species, thereby reducing the reduction temperature of Cu^{2+} species in the NC-CuMgAlO. Additionally, as shown in Table S1, the actual amount of H_2 consumption determined by H_2-TPR follows the order of NC-CuAlO (5.82 mmol/g) > CuMgAlO (4.46 mmol/g) > NC-CuMgAlO (3.82 mmol/g), which is in good accordance with the order of copper loading in samples. Moreover, the theoretical H_2 consumption for NC-CuAlO, CuMgAlO and NC-CuMgAlO calculated based on the complete reduction of Cu^{2+} to Cu^0 is 6.67, 5.08 and 4.94 mmol/g, respectively. The lower amounts of actual H_2 consumption than the theoretical values are correlated with the presence of Cu^+ species in reduced Cu-based samples.

CO_2-TPD measurements were carried out to achieve information on the surface basicity of different Cu-based samples. As shown in Fig. 4, the broad CO_2 desorption peak can be fitted into five different peaks in each case, which are assigned to weak Brønsted basic sites (W.) centered at 90 °C, medium-strength basic sites (M.) centered at 275 °C, strong basic sites (S.) centered at 404 °C and 492 °C, and super strong basic sites (SS.) centered at 581 °C on the surface, respectively. Moreover, the amounts and proportions of different kinds of basic sites are

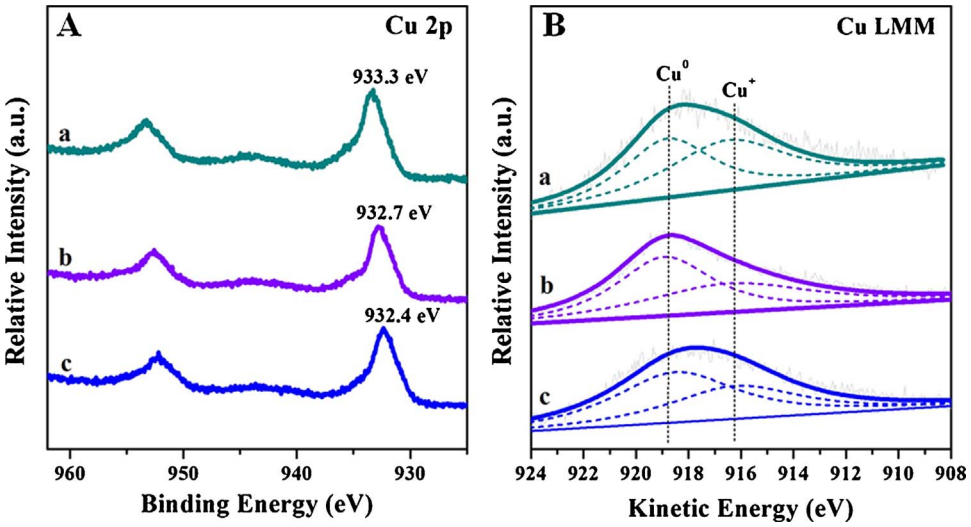

Fig. 5. XPS (A) of Cu 2p region and Cu LMM XAES (B) for NC-Cu/MgAlO (a), NC-Cu/Al_2O_3 (b) and Cu/MgAlO (c) samples.

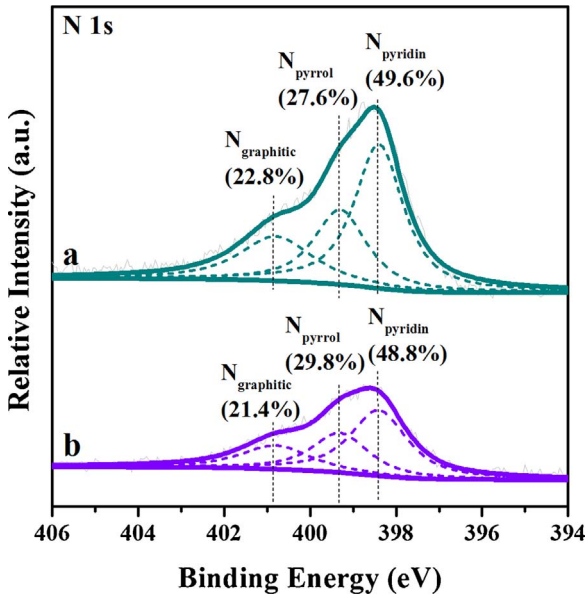

Fig. 6. Fine N 1 s XPS of NC-Cu/Al_2O_3 (a) and NC-Cu/MgAlO (b).

Table 3
The catalytic transfer hydrogenolysis of HMF over different catalysts.[a]

Catalyst	Conv. (%)	Selectivity (%)					TOF[c] (h^{-1})
		DMF	5-MFA	BHMF	DMTHF	Others[b]	
NC-Cu/MgAlO	100	96.1	0	0	3.3	0.6	238.6
Cu/MgAlO	94.7	75.6	20.5	0	2.9	1.0	195.1
NC-Cu/Al_2O_3	85.2	80.4	16.1	0	2.7	0.8	165.8
NC-MgAlO	100	0	0	100	0	0	–

[a] Reaction conditions: catalysts, 0.1 g; HMF, 0.5 g; cyclohexanol, 10 mL; reaction time, 30 min; reaction temperature, 220 °C; N_2 atmosphere.
[b] Others mainly include 5-methylfurfural and 5-methyltetrahydrofurfuryl alcohol.
[c] Calculated based on the moles of HMF converted per mole surface metallic copper in the initial 10 min.

determined based on integrated peak areas (Table 2). It can be found that compared with other two samples, NC-Cu/MgAlO possesses a larger amount of total basic sites. Noticeably, the amounts of weak basic sites are similar in three samples, while the amount of medium-strength basic sites in the NC-Cu/MgAlO is the lowest. Interestingly, among three samples, NC-Cu/MgAlO possesses the highest amount of strong basic sites and super strong basic sites, mirroring that the introduction of both Mg and NC significantly promotes the formation of surface super strong basic sites. Further, in situ IR spectra of pyridine adsorption over different Cu-based samples show that there are two broad bands from physically adsorbed pyridine at about 1438 cm^{-1} and 1588 cm^{-1} [49] (Fig.S3). And, two very weak bands related to pyridine adsorption on Lewis acid sites (1455 cm^{-1}) and Brønsted acid sites (1542 cm^{-1}) are detected [50]. While NH_3-TPD profiles of different samples only present one desorption peak at about 135 °C, which is associated with weak acid sites [51], and the difference in surface acid density is very small (Table S2). The aforementioned results illustrate that surface acidity of different Cu-based samples is weak, and the difference in surface acidity is not significant.

To further gain insight into the metal-support interactions, XPS characterization was performed. From the fine Cu 2p spectra (Fig. 5A), it can be seen that the binding energy (BE) of Cu^0 species for NC-Cu/MgAlO is about 933.3 eV. The higher BE value than those for NC-Cu/Al_2O_3 (932.7 eV) and Cu/MgAlO (932.4 eV) is attributable to the formation of strong metal-support interactions (SMSIs), thereby leading to the electron transfer from Cu species to NC and MMO components. However, the satellite peak of Cu^{2+} species at 942–944 eV is hardly observed in all cases, demonstrating the complete reduction of Cu^{2+} species. To further determine the chemical states of Cu species, Cu XAES spectra was analyzed. As shown in Fig. 5B, two deconvoluted peaks at the kinetic energy of about 916.3 and 918.7 eV correspond to Cu^+ and Cu^0 species, respectively [52,53]. Notably, NC-Cu/MgAlO possesses the largest surface $Cu^+/(Cu^0 + Cu^+)$ molar ratio (0.54) (Table 1), suggesting the formation of SMSIs in the forms of possible Cu^+-O-M (M = Mg or Al) or Cu^+-NC modes [54].

The types and contents of different N species on the surface of NC-Cu/Al_2O_3 and NC-Cu/MgAlO were determined by XPS. As shown in Fig. 6, the N 1 s spectra can be deconvoluted into three different contributions at about 398.4, 399.3 and 400.8 eV, respectively, which are assigned to pyridinic-N atoms, pyrrolic-N atoms and graphitic-N atoms [55–57]. It implies that N atoms are successfully doped into the carbon framework, in accordance with the above HAADF-STEM-EDS results. Correspondingly, these electron-rich N sites can generate plentiful Lewis basic sites, which are believed to be able to facilitate transfer hydrogenation reactions [58,59]. In addition, it is seen that the contents of different types of N atoms in samples are different. Specially, the content of pyrrolic-N atoms for NC-Cu/MgAlO is slightly higher than that for NC-Cu/Al_2O_3. It was reported that such pyrrolic-N atoms might improve the metal dispersion in some cases [60], probably influencing

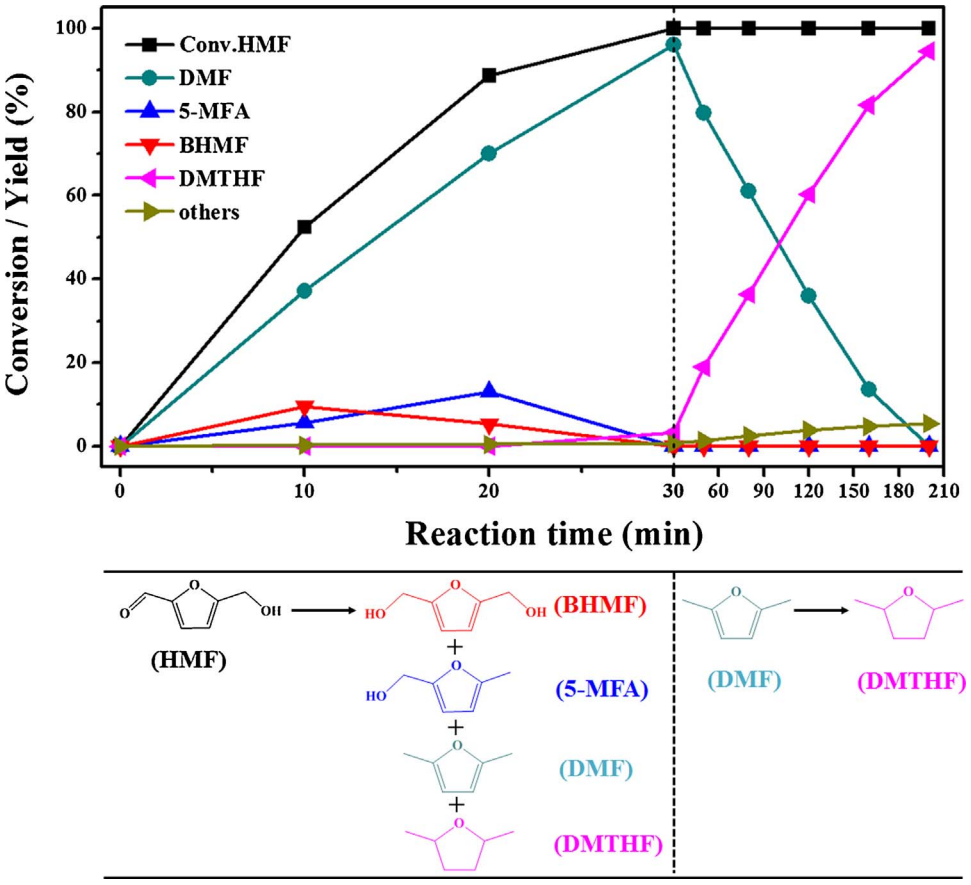

Fig. 7. The effect of reaction time on the transfer hydrogenolysis of HMF. Reaction conditions: NC-Cu/MgAlO, 0.1 g; HMF, 0.5 g; cyclohexanol, 10 mL; N_2 atmosphere; reaction temperature, 220 °C. Others mainly include 2-methylfuran, tetrahydrofuran and C—C cracking products.

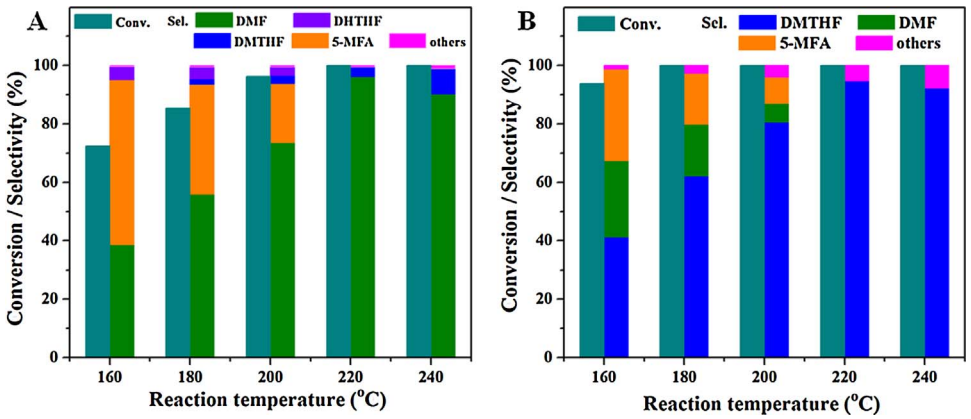

Fig. 8. The effect of reaction temperature on the transfer hydrogenolysis of HMF after a reaction time of 30 min (A) or 200 min (B). Reaction conditions: NC-Cu/MgAlO, 0.1 g; HMF, 0.5 g; cyclohexanol, 10 mL; N_2 atmosphere.

the catalytic activity of catalysts.

3.3. Catalytic transfer hydrogenolysis of HMF

The catalytic performance of different catalysts was investigated in the liquid-phase transfer hydrogenolysis of HMF and the catalytic results are summarized in Table 3. When using NC-Cu/MgAlO, a complete conversion with a high DMF yield of 96.1% is achieved at 220 °C only after a reaction time of 30 min, indicative of the excellent catalytic performance of NC-Cu/MgAlO. In contrast, NC-Cu/Al_2O_3 and Cu/MgAlO gain HMF conversions of 85.2% and 94.7%, respectively, along with low selectivities to furanic fuels (DMF or DMTHF). In two cases, the major byproduct is 5-MFA, indicating the poor hydrogenolysis ability of NC-Cu/Al_2O_3 and Cu/MgAlO. Furthermore, as shown in Fig. S4, the HMF conversion over the NC-Cu/MgO is only 80.3% after a reaction of 30 min, indicative of the poor catalytic performance compared with NC-Cu/MgAlO, NC-Cu/Al_2O_3 and Cu/MgAlO, probably due to the larger particle size of Cu NPs in the NC-Cu/MgO (Fig.S2). Notably, over the Cu-free NC-MgAlO comparison sample, HMF is totally converted to BHMF without the formation of DMF and DMTHF, proving that Cu species are actual active sites for the hydrogenolysis of hydroxyl group in HMF. In addition, compared with other Cu-, Ru- and Pd-based catalysts reported previously in the literature [13,23,26–28,61] (Table S3), the present NC-Cu/MgAlO exhibits a comparable or higher catalytic performance for the transfer hydrogenation of HMF, despite different reaction conditions.

To obtain the intrinsic activity of different catalysts, the turnover frequency (TOF) value was calculated based on the moles of HMF converted per mole surface metallic copper in the initial 10 min. As shown in Table 3, the TOF value for NC-Cu/MgAlO is as high as about 238.6 h^{-1}, higher than those for Cu/MgAlO and NC-Cu/Al_2O_3, strongly reflecting the higher catalytic efficiency of NC-Cu/MgAlO in the

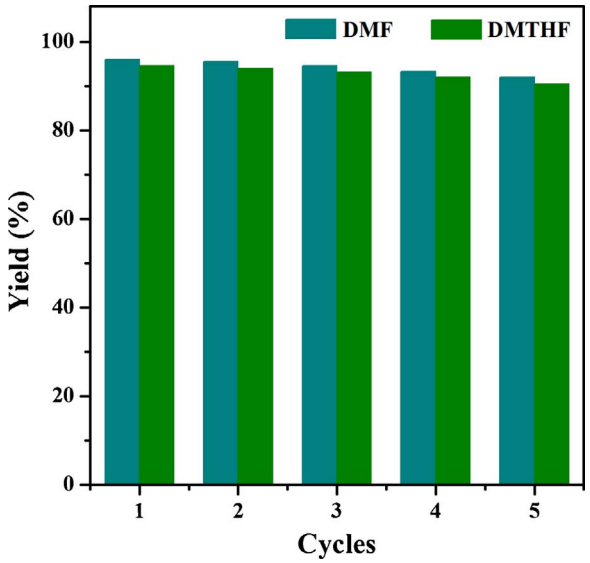

Fig. 9. The reusability of NC-Cu/MgAlO catalyst in the transfer hydrogenolysis of HMF. Reaction conditions: catalyst, 0.1 g; HMF, 0.5 g; cyclohexanol, 10 mL; reaction temperature, 220 °C; reaction time, 30 min (dark cyan) or 200 min (olive); N_2 atmosphere.

catalytic transfer hydrogenolysis of HMF.

Further, Fig. 7 reveals the influence of reaction time on the HMF transfer hydrogenolysis at 220 °C. Noticeably, the HMF conversion increases monotonously with the reaction time within 30 min, whereas the DMF yield increases approximately linearly. Meanwhile, BHMF or 5-MFA yields firstly increase with the reaction time in the initial 10 min or 20 min and then decrease along with the reaction time. Further increasing the reaction time leads to a continuous transformation of DMF to DMTHF. Finally, a high DMTHF yield of 94.6% is achieved after a reaction time of 200 min. The above results demonstrate the synthesis of DMF or DMTHF can be diversely achieved only through simply modulating the reaction time over the NC-Cu/MgAlO catalyst. As a result, the time-course analysis for the conversion of HMF clearly indicates a tandem reaction pathway for the conversion of HMF to DMF via BHMF and MFA over the NC-Cu/MgAlO catalyst and following transformation of DMF into DMTHF. Also, the hydrogenation of DMF as initial reactant was conducted (Fig. S5). Noticeably, DMF is gradually converted to DMTHF with the increasing reaction time, further demonstrating the convertible production of DMF and DMTHF in the present catalytic system.

The transfer hydrogenolysis of HMF to produce DMF was also studied using different hydrogen donors over the NC-Cu/MgAlO. As listed in Table S4, the hydrogen donor can greatly influence the transfer hydrogenolysis of HMF, which should be ascribed to different reduction potentials of alcohols. The alcohol owing high reduction potential is hard to be oxidized, meaning that the dehydrogenation is difficult. Previously, van der Waal et al. reported that the reduction potentials of alcohols follows the order of 2-propanol ≈ 2-butanol < 1-butanol < ethanol < methanol [62]. The reduction potential of methanol is much higher than other alcohols, which results in a lower HMF conversion. In contrast, secondary alcohols (i.e. 2-butanol and 2-propanol) with lower reduction potentials than primary alcohols can yield higher HMF conversions. Interestingly, the DMF selectivity does not obviously change with different alcohols, because the DMF selectivity is mainly related to the applied catalytic systems.

The influence of reaction temperature on the transfer hydrogenolysis of HMF was explored. As shown in Fig. 8A, the reaction temperature greatly impacts both the HMF conversion and DMF selectivity after a reaction time of 30 min. Upon increasing the temperature from 160 to 220 °C, the HMF conversion increases gradually from 72.4 to 100% and the DMF selectivity quickly increases from 38.7 to 96.1%. Meanwhile, 5-MFA, as dominant byproduct, is dramatically converted to DMF with the reaction temperature. It demonstrates that the high temperature can accelerate the hydrogenolysis of hydroxyl group in HMF and 5-MFA. Moreover, a slow increase in the DMTHF selectivity with increasing reaction temperature illustrates that the hydrogenation of furan ring can be promoted at relatively high reaction temperature. As presented in Fig. 8B, the reaction temperature also has an obvious effect on the products selectivity after a reaction time of 200 min. Along with the increase of reaction temperature, the DMTHF selectivity increases gradually with the decrease of DMF and 5-MFA selectivity. The selectivity of DMTHF at 240 °C is lower than that at 220 °C because of the excess formation of byproducts.

The reusability of the NC-Cu/MgAlO catalyst was tested for the transfer hydrogenolysis of HMF. After reaction, the reaction mixture was centrifuged and the catalyst was collected, washed with deionized water and ethyl alcohol for three times, dried at 70 °C for 12 h and finally used for next run. It is noticed that the DMF and DMTHF yields only decrease by about 4.2% and 4.3%, respectively, after five consecutive runs (Fig. 9). The reaction filtrate after five consecutive cycles was determined by ICP-AES and the result reveals a negligible leaching of Cu species. Moreover, from TEM images of used catalysts after five runs in two different reaction conditions and particle size distribution histograms of Cu NPs estimated based on TEM images (Fig. S6), we can find that the particle size of Cu NPs slightly increases from 4.59 to 5.14 nm in the reaction time of 30 min and 5.49 nm in the reaction time of 200 min. Moreover, the Cu LMM XAES spectrum of used NC-Cu/MgAlO after reaction was further analyzed (Fig. S7) and the result indicates that the $Cu^+/(Cu^0 + Cu^+)$ molar ratio almost keeps unchanged

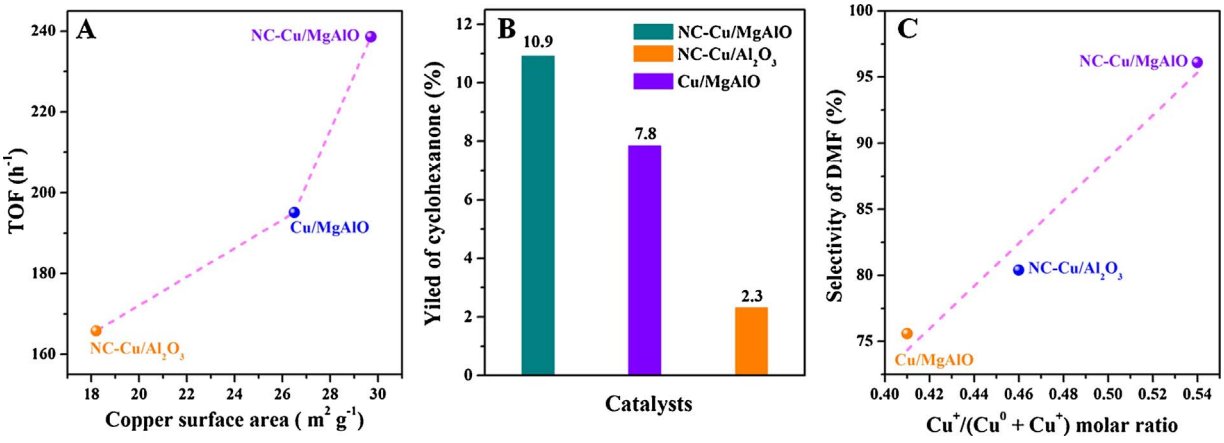

Fig. 10. (A) The TOF value as functions of the copper surface area in different catalysts; (B) Change in the yield of cyclohexanone with different samples. Conditions: catalysts, 0.1 g; cyclohexanol, 10 mL; reaction time, 30 min; reaction temperature, 220 °C; N_2 atmosphere; (C) The selectivity of DMF as functions of the $Cu^+/(Cu^0 + Cu^+)$ ratio for different catalysts.

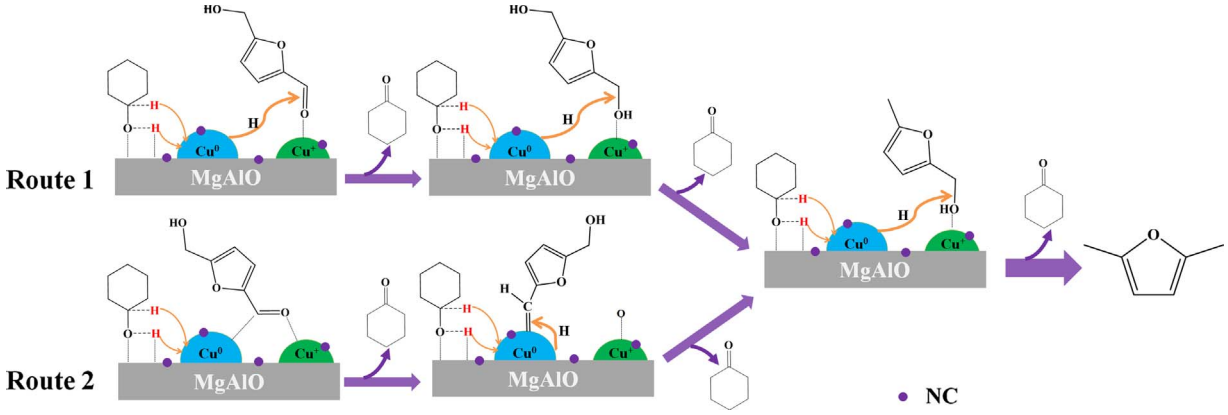

Scheme 2. Proposed possible mechanism for the hydrogenolysis process of HMF to produce DMF over the NC-Cu/MgAlO catalyst through two reaction routes.

after reaction. Above results strongly reflect the good stability and reusability of the present NC-Cu/MgAlO catalyst.

3.4. Mechanical study on catalytic transfer hydrogenolysis

Generally, the catalytic activity of supported metal catalysts is strongly related to their microstructure of catalysts, such as active metal surface area and metal–support interactions. Commonly, the high active metal surface area of catalysts is responsible for the high catalytic activity. As shown in Fig. 10A, the variation of the TOF value as a function of the Cu surface area in different catalysts are presented to explore the relationship between them. It can be noticed that the high copper surface area is beneficial to the improvement of the catalytic activity. However, the TOF value does not correlate linearly with the copper surface area, indicating that the copper surface area is not the sole key factor influencing the catalytic activity in the present catalytic system.

On the other side, for catalytic transfer hydrogenolysis, easy dehydrogenation of cyclohexanol can promote the transformation of HMF. Therefore, the dehydrogenation ability of different catalysts was investigated to further explore the origin of catalytic activity of catalysts. As shown in Fig. 10B, in the absence of HMF substrate, the cyclohexanone yield increases in the following order of NC-Cu/Al_2O_3 < Cu/MgAlO < NC-Cu/MgAlO, well consistent with the order of the amount of surface base sites in three samples. This result strongly proves that the larger amount of surface strong base sites in the NC-Cu/MgAlO can facilitate the dehydrogenation of cyclohexanol, thus leading to high activity in the catalytic transfer hydrogenolysis of HMF. In addition, due to slight difference in surface acidic site density, as well as very small amounts of acidic sites, surface acidity of the present catalyst system may be not a critical factor in improving HMF conversion, despite the fact that Lewis acid sites have been proposed as active sites for catalytic hydrogen transfer via Meerwein-Ponndorf-Verley reduction. Therefore, it can be reasonably concluded that the high activity of NC-Cu/MgAlO should be closely related to surface cooperation between copper surface area and base sites.

In addition, in order to find out the intrinsic reason for different selectivities in different samples, the correlation between the DMF selectivity and the $Cu^+/(Cu^0 + Cu^+)$ molar ratio is shown in Fig. 10C. It is interesting to find that the DMF selectivity approximately increases linearly with the increasing $Cu^+/(Cu^0 + Cu^+)$ molar ratio. This result implies that the high $Cu^+/(Cu^0 + Cu^+)$ molar ratio may contribute to the hydrogenolysis of hydroxyl group in BHMF and 5-MFA, thereby leading to high selectivity to DMF.

Based on above structural characterization and catalytic test results, a plausible reaction mechanism for the liquid-phase catalytic transfer hydrogenolysis of HMF to produce DMF over the NC-Cu/MgAlO catalyst is proposed (Scheme 2). For the dehydrogenation of cyclohexanol, firstly, the hydroxyl group in cyclohexanol may interact with active basic sites on the catalyst surface, and then the hydrogen atom in alcoholic group can be abstracted to form adsorbed alkoxide species. Subsequently, the β-H atom can be further removed to generate cyclohexanone. Meanwhile, active hydrogen species formed can further involve the HMF hydrogenolysis. For the hydrogenolysis process, in the case of reaction route 1, the carbonyl oxygen of HMF that has lone pair electrons firstly adsorbs on electrophilic Cu^+ species, which will promote the activation of the C═O bond. Then, the hydrogenation of the carbonyl group in HMF is induced by Cu NPs using the abstracted hydrogen, leading the formation of BHMF. Then, surface electrophilic Cu^+ species, serving as Lewis acid sites, can facilitate the polarization and activation of the C−O bond in BHMF and 5-MFA, finally leading to the production of DMF with the help of Cu NPs. In the case of reaction route 2, the C═O bond in HMF may firstly adsorb onto the surface via an η^2(C,O) configuration, where the C atom is bonded to metallic Cu NP and the O atom is bonded to Cu^+ species, thereby leading to the formation of CH_2OH-(C_4H_2O)−CH = intermediate on the surface of Cu NPs [63]. Subsequently, the intermediate can be hydrogenated to form 5-MFA by active hydrogen species released from cyclohexanol dehydrogenation. Finally, like the reaction route 1, the hydrogenolysis of hydroxyl group in 5-MFA to DMF can take place with the help of electrophilic Cu^+ species and metallic Cu NPs. As a result, the high catalytic performance of NC-Cu/MgAlO in the catalytic transfer hydrogenolysis HMF to DMF is mainly ascribed to the cooperation between surface base sites and Cu species (Cu^0 and Cu^+ species), which can efficiently promote the dehydrogenation of cyclohexanol and subsequent hydrogenolysis of HMF.

4. Conclusions

In summary, a high-performance and stable Cu-based catalyst was developed by a facile thermal decomposition of CuMgAl-LDH/melamine hybrid precursor and employed for the transfer hydrogenolysis of HMF to produce DMF or DMTHF. HMF could be totally converted to DMF with a high yield of 96.1% only after a reaction time of 30 min at 220 °C. A further reaction of 170 min resulted in the production of DMTHF with a high yield of 94.6%. A series of characterization and experimental results revealed that the cooperation between abundant surface basic sites and highly dispersed Cu species was mainly attributable to the realization of high catalytic performance of the catalyst. Correspondingly, three key factors (i.e. surface basic sites, Cu^0 NPs and Cu^+ species) could efficiently and cooperatively govern the hydrogenolysis of HMF and dehydrogenation of cyclohexanol. Moreover, the strong interaction between Cu NPs and the support could significantly prevent the aggregation of Cu NPs and thus greatly enhance the stability of the catalyst. The attractive feature of the present copper-based catalyst provides a guiding principle for future catalyst design in the

field of biomass conversion.

Acknowledgments

We gratefully thank the financial support from National Natural Science Foundation of China (21325624; 21521005; 21776017) and the Fundamental Research Funds for the Central Universities (buctrc201528).

Appendix A. Supplementary data

Supplementary data associated with this article can be found, in the online version, at https://doi.org/10.1016/j.apcatb.2018.01.006.

References

[1] L.S. Ribeiro, J.J. Delgado, J.J.M. Órfão, M.F.R. Pereira, Carbon supported Ru-Ni bimetallic catalysts for the enhanced one-pot conversion of cellulose to sorbitol, Appl. Catal. B: Environ. 217 (2017) 265–274.
[2] L.S. Ribeiro, J.J.M. Órfão, M.F.R. Pereira, Enhanced direct production of sorbitol by cellulose ball-milling, Green Chem. 17 (2017) 2973–2980.
[3] A.J. Ragauskas, C.K. Williams, B.H. Davison, G. Britovsek, J. Cairney, C.A. Eckert, W.J. Frederick, J.P. Hallett, D.J. Leak, C.L. Liotta, The path forward for biofuels and biomaterials, Science 311 (2006) 484–489.
[4] C. Aellig, P.D.I. Hermans, Continuous D-Fructose dehydration to 5-hydroxymethylfurfural under mild conditions, ChemSusChem 5 (2012) 1737–1742.
[5] N. Shi, Q. Liu, Q. Zhang, T. Wang, L. Ma, High yield production of 5-hydroxymethylfurfural from cellulose by high concentration of sulfates in biphasic system, Green Chem. 15 (2013) 1967–1974.
[6] J.N. Chheda, Y. Roman-Leshkov, J.A. Dumesic, Production of 5-hydroxymethylfurfural and furfural by dehydration of biomass-derived mono- and polysaccharides, Green Chem. 9 (2007) 342–350.
[7] Y. Román-Leshkov, C.J. Barrett, Z.Y. Liu, J.A. Dumesic, Production of dimethylfuran for liquid fuels from biomass-derived carbohydrates, Nature 447 (2007) 982–986.
[8] W. Yang, A. Sen, One-step catalytic transformation of carbohydrates and cellulosic biomass to 2,5-dimethyltetrahydrofuran for liquid fuels, ChemSusChem 3 (2010) 597–603.
[9] T. Ståhlberg, W.J. Fu, J.M. Woodley, A. Riisager, Synthesis of 5-(hydroxymethyl) furfural in ionic liquids: paving the way to renewable chemicals, ChemSusChem 4 (2011) 451–458.
[10] G.-H. Wang, J. Hilgert, F.H. Richter, F. Wang, H.-J. Bongard, B. Spliethoff, C. Weidenthaler, F. Schüth, Platinum–cobalt bimetallic nanoparticles in hollow carbon nanospheres for hydrogenolysis of 5-hydroxymethylfurfural, Nat. Mater. 13 (2014) 293–300.
[11] T. Thananatthanachon, T.B. Rauchfuss, Efficient production of the liquid fuel 2,5-dimethylfuran from fructose using formic acid as a reagent, Angew. Chem. 122 (2010) 6766–6768.
[12] L. Hu, X. Tang, J.X. Xu, Z. Wu, L. Lin, S.J. Liu, Selective transformation of 5-hydroxymethylfurfural into the liquid fuel 2,5-dimethylfuran over carbon-supported ruthenium, Ind, Eng. Chem. Res. 53 (2014) 3056–3064.
[13] Y.H. Zu, P.P. Yang, J.J. Wang, X.H. Liu, J.W. Ren, G.Z. Lu, Y.Q. Wang, Efficient production of the liquid fuel 2,5-dimethylfuran from 5-hydroxymethylfurfural over Ru/Co_3O_4 catalyst, Appl. Catal. B: Environ. 146 (2014) 244–248.
[14] A.S. Nagpure, A.K. Venugopal, N. Lucas, M. Manikandan, R. Thirumalaiswamy, S. Chilukuri, Renewable fuels from biomass-derived compounds: Ru-containing hydrotalcites as catalysts for conversion of HMF to 2,5-dimethylfuran, Catal. Sci. Technol. 5 (2015) 1463–1472.
[15] Y. Nakagawa, K. Takada, M. Tamura, K. Tomishige, Total hydrogenation of furfural and 5-hydroxymethylfurfural over supported Pd-Ir alloy catalyst, ACS Catal. 4 (9) (2014) 2718–2726.
[16] M. Chatterjee, T. Ishizaka, H. Kawanami, Hydrogenation of 5-hydroxymethylfurfural in supercritical carbon dioxide–water: a tunable approach to dimethylfuran selectivity, Green Chem. 16 (2014) 1543–1551.
[17] M. Chidambaram, A.T. Bell, A two-step approach for the catalytic conversion of glucose to 2,5-dimethylfuran in ionic liquids, Green Chem. 12 (2010) 1253–1262.
[18] X. Kong, R.X. Zheng, Y.F. Zhu, G.Q. Ding, Y.L. Zhu, Y.-W. Li, Rational design of Ni-based catalysts derived from hydrotalcite for selective hydrogenation of 5-hydroxymethylfurfural, Green Chem. 17 (2015) 2504–2514.
[19] X. Kong, Y.F. Zhu, H.Y. Zheng, X.Q. Li, Y.L. Zhu, Y.-W. Li, Ni nanoparticles inlaid nickel phyllosilicate as a metal-acid bifunctional catalyst for low-temperature hydrogenolysis reactions, ACS Catal. 5 (2015) 5914–5920.
[20] Y.-B. Huang, M.-Y. Chen, L. Yan, Q.-X. Guo, Y. Fu, Nickel–tungsten carbide catalysts for the production of 2,5-dimethylfuran from biomass-derived molecules, ChemSusChem 7 (2014) 1068–1070.
[21] P.P. Yang, Q.Q. Cui, Y.H. Zu, X.H. Liu, G.Z. Lu, Y.Q. Wang, Catalytic production of 2,5-dimethylfuran from 5-hydroxymethylfurfural over Ni/Co_3O_4 catalyst, Catal. Commun. 66 (2015) 55–59.
[22] G. Bottari, A.J. Kumalaputri, K.K. Krawczyk, B.L. Feringa, H.J. Heeres, K. Barta, Copper–zinc alloy nanopowder: a robust precious-metal-free catalyst for the conversion of 5-hydroxymethylfurfural, ChemSusChem 8 (2015) 1323–1327.
[23] B. Chen, F. Li, Z. Huang, G. Yuan, Carbon-coated Cu-Co bimetallic nanoparticles as selective andrecyclable catalysts for production of biofuel 2,5-dimethylfuran, Appl. Catal. B: Environ. 200 (2017) 192–199.
[24] W.W. Guo, H.Y. Liu, S.Q. Zhang, H.L. Han, H.Z. Liu, T. Jiang, B.X. Han, T.B. Wu, Efficient hydrogenolysis of 5-hydroxymethylfurfural to 2,5-dimethylfuran over a cobalt and copper bimetallic catalyst on N-graphene-modified Al_2O_3, Green Chem. 18 (2016) 6222–6228.
[25] M.M. Wright, D.E. Daugaard, J.A. Satrio, R.C. Brown, Techno-economic analysis of biomass fast pyrolysis to transportation fuels, Fuel 89 (2010) S2–S10.
[26] J. Jae, W.Q. Zheng, R.F. Lobo, D.G. Vlachos, Production of dimethylfuran from hydroxymethylfurfural through catalytic transfer hydrogenation with Ruthenium supported on carbon, ChemSusChem 6 (2013) 1158–1162.
[27] D. Scholz, C. Aellig, I. Hermans, Catalytic transfer hydrogenation/hydrogenolysis for reductive upgrading of furfural and 5-(hydroxymethyl) furfural, ChemSusChem 7 (2014) 268–275.
[28] J. Mitra, X.Y. Zhou, T. Rauchfuss, Pd/C-catalyzed reactions of HMF: decarbonylation, hydrogenation, and hydrogenolysis, Green Chem. 17 (2015) 307–313.
[29] J. Jae, W.Q. Zheng, A.M. Karim, K. Guo, R.F. Lobo, D.G. Vlachos, The role of Ru and RuO_2 in the catalytic transfer hydrogenation of 5-hydroxymethylfurfural for the production of 2,5-dimethylfuran, ChemCatChem 6 (2014) 848–856.
[30] P.J. Sideris, U.G. Nielsen, Z.H. Gan, C.P. Grey, Mg/Al ordering in layered double hydroxides revealed by multinuclear NMR spectroscopy, Science 321 (2008) 113–117.
[31] A.I. Tsyganok, T. Tsunoda, S. Hamakawa, K. Suzuki, K. Takehira, T. Hayakawa, Dry reforming of methane over catalysts derived from nickel-containing Mg–Al layered double hydroxides, J. Catal. 213 (2003) 191–203.
[32] C. Gérardin, D. Kostadinova, N. Sanson, B. Coq, D. Tichit, Supported metal particles from LDH nanocomposite precursors: control of the metal particle size at increasing metal content, Chem. Mater. 17 (2005) 6473–6478.
[33] C. Gérardin, D. Kostadinova, B. Coq, D. Tichit, LDH nanocomposites with different guest entities as precursors of supported Ni catalysts, Chem. Mater. 20 (2008) 2086–2094.
[34] E.M. Albuquerque, L.E.P. Borges, M.A. Fraga, Lactic acid production from hydroxyacetone on dual metal/base heterogeneous catalytic systems, Green Chem. 17 (2015) 3889–3899.
[35] M. Zhang, Y.J. Zhao, Q. Liu, L. Yang, G.L. Fan, F. Li, A La-doped Mg-Al mixed metal oxide supported copper catalyst with enhanced catalytic performance in transfer dehydrogenation of 1-decanol, Dalton Trans. 45 (2016) 1093–1102.
[36] M.J. Climent, A. Corma, S. Iborra, K. Epping, A. Velty, Increasing the basicity and catalytic activity of hydrotalcites by different synthesis procedures, J. Catal. 225 (2004) 316–326.
[37] E. Li, Z.P. Xu, V. Rudolph, MgCoAl–LDH derived heterogeneous catalysts for the ethanol transesterification of canola oil to biodiesel, Appl. Catal. B: Environ. 88 (2009) 42–49.
[38] Q. Hu, G.L. Fan, L. Yang, X.Z. Cao, P. Zhang, B.Y. Wang, F. Li, A gas-phase coupling process for simultaneous production of γ-butyrolactone and furfuryl alcohol without external hydrogen over bifunctional base-metal heterogeneous catalysts, Green Chem. 18 (2016) 2317–2322.
[39] Y.W. Zhu, S. Murali, M.D. Stoller, K.J. Ganesh, W.W. Cai, P.J. Ferreira, A. Pirkle, R.M. Wallace, K.A. Cychosz, M. Thommes, D. Su, E.A. Stach, R.S. Ruoff, Carbon-based supercapacitors produced by activation of graphene, Science 332 (2011) 1537–1541.
[40] S.B. Yang, X.L. Feng, X.C. Wang, K. Müllen, Graphene-based carbon nitride nanosheets as efficient metal-free electrocatalysts for oxygen reduction reactions, Angew. Chem. Int. Ed. 50 (2011) 5339–5343.
[41] J.S. Lee, X.Q. Wang, H.M. Luo, G.A. Baker, S. Dai, Facile ionothermal synthesis of microporous and mesoporous carbons from task specific ionic liquids, J. Am. Chem. Soc. 131 (2009) 4596–4597.
[42] Z.S. Ma, H.Y. Zhang, Z.Z. Yang, G.P. Ji, B. Yu, X.W. Liu, Z.M. Liu, Mesoporous nitrogen-doped carbons with high nitrogen contents and ultrahigh surface areas: synthesis and applications in catalysis, Green Chem. 18 (2016) 1976–1982.
[43] J. Wei, D.D. Zhou, Z.K. Sun, Y.H. Deng, Y.Y. Xia, D.Y. Zhao, A controllable synthesis of rich nitrogen-doped ordered mesoporous carbon for CO_2 capture and supercapacitors, Adv. Funct. Mater. 23 (2013) 2322–2328.
[44] W. Yang, T.-P. Fellinger, M. Antonietti, Efficient metal-free oxygen reduction in alkaline medium on high-surface-area mesoporous nitrogen-doped carbons made from ionic liquids and nucleobases, J. Am. Chem. Soc. 133 (2011) 206–209.
[45] Y.Y. Shao, J.H. Sui, G.P. Yin, Y.Z. Gao, Nitrogen-doped carbon nanostructures and their composites as catalytic materials for proton exchange membrane fuel cell, Appl. Catal. B: Environ. 79 (2008) 89–99.
[46] Y. Zheng, J. Liu, J. Liang, M. Jaroniec, S.Z. Qiao, Graphitic carbon nitride materials: controllable synthesis and applications in fuel cells and photocatalysis, Energy Environ. Sci. 5 (2012) 6717–6731.
[47] R.F. Nie, H.H. Yang, H.F. Zhang, X.L. Yu, X.H. Lu, D. Zhou, Q.H. Xia, Mild-temperature hydrodeoxygenation of vanillin over porous nitrogen-doped carbon black supported nickel nanoparticles, Green Chem. 19 (2017) 3126–3134.
[48] X.H. Liu, L.J. Xu, G.Y. Xu, W.D. Jia, Y.F. Ma, Y. Zhang, Selective hydrodeoxygenation of lignin-derived phenols to cyclohexanols or cyclohexanes over magnetic CoN_x@NC catalysts under mild conditions, ACS Catal. 6 (2016) 7611–7620.
[49] B. Tang, W.L. Dai, G.G. Wu, N.J. Guan, L.D. Li, M. Hunger, Improved postsynthesis strategy to Sn-Beta zeolites as lewis acid catalysts for the ring-opening hydration of epoxides, ACS Catal. 4 (2014) 2801–2810.
[50] E.P. parry, An infrared study of pyridi, ne adsorbed on acidic solids. Characterization of surface acidity, J. Catal. 2 (1963) 371–379.
[51] H. Xu, Q. Zhang, C. Qiu, T. Lin, M. Gong, Y. Chen, Tungsten modified MnO_x–CeO_2/

ZrO_2 monolith catalysts for selective catalytic reduction of NO_x with ammonia, Chem. Eng. Sci. 76 (2012) 120–128.
[52] Q. Hu, G.L. Fan, S.Y. Zhang, L. Yang, F. Li, Gas phase hydrogenation of dimethyl-1,4-cyclohexane dicarboxylate over highly dispersed and stable supported copper-based catalysts, J. Mol. Catal. A: Chem. 397 (2015) 134–141.
[53] Z. He, H.Q. Lin, P. He, Y.Z. Yuan, Effect of boric oxide doping on the stability and activity of a Cu–SiO_2 catalyst for vapor-phase hydrogenation of dimethyl oxalate to ethylene glycol, J. Catal. 277 (2011) 54–63.
[54] W.-J. Lee, Y.-S. Lee, S.-K. Rha, Y.-J. Lee, K.-Y. Lim, Y.-D. Chung, C.-N. Whange, Adhesion and interface chemical reactions of Cu/polyimide and Cu/TiN by XPS, Appl. Surf. Sci. 205 (2003) 128–136.
[55] S. Chen, J.Y. Bi, Y. Zhao, L.J. Yang, C. Zhang, Y.W. Ma, Q. Wu, X.Z. Wang, Z. Hu, Nitrogen-doped carbon nanocages as efficient metal-free electrocatalysts for oxygen reduction reaction, Adv. Mater. 24 (2012) 5593–5597.
[56] T. Sharifi, G.Z. Hu, X. Jia, T. Wagberg, Formation of active sites for oxygen reduction reactions by transformation of nitrogen functionalities in nitrogen-doped carbon nanotubes, ACS. Nano. 6 (2012) 8904–8912.
[57] J.L. Long, X.Q. Xie, J. Xu, Q. Gu, L.M. Chen, X.X. Wang, Nitrogen-doped graphene nanosheets as metal-free catalysts for aerobic selective oxidation of benzylic alcohols, ACS Catal. 2 (2012) 622–631.
[58] J.L. Long, B.L. Yin, Y.W. Li, L.J. Zhang, Selective hydrogenation of nitriles to imines over a multifunctional heterogeneous Pt catalyst, AIChE J. 60 (2014) 3565–3576.
[59] R. Noyori, M. Yamakawa, S. Hashiguchi, Metal-ligand bifunctional catalysis: a nonclassical mechanism for asymmetric hydrogen transfer between alcohols and carbonyl compounds, J. Org. Chem. 66 (2001) 7931–7944.
[60] W.W. Guo, H.Y. Liu, S.Q. Zhang, H.L. Han, H.Z. Liu, T. Jiang, B.X. Han, T.B. Wu, Efficient hydrogenolysis of 5-hydroxymethylfurfural to 2,5-dimethylfuran over a cobalt and copper bimetallic catalyst on N-graphene-modified Al_2O_3, Green Chem. 18 (2016) 6222–6228.
[61] T.S. Hansen, K. Barta, P.T. Anastas, P.C. Ford, A. Riisager, One-pot reduction of 5-hydroxymethylfurfural via hydrogen transfer from supercritical methanol, Green Chem. 14 (2012) 2457–2461.
[62] J.C. van der Waal, P.J. Kunkeler, K. Tan, H. van Bekkum, Zeolite titanium beta: a selective catalyst for the gas-phase Meerwein–Ponndorf–Verley, and Oppenauer reactions, J. Catal. 173 (1998) 74–83.
[63] D.M. Shi, J.M. Vohs, Deoxygenation of biomass-derived oxygenates: reaction of furfural on Zn-modified Pt(111), ACS Catal. 5 (2015) 2177–2183.